THE JOURNAL OF PHYSICAL CHEMISTRY Letters

Letter

pubs.acs.org/JPCL

Energy Band Alignment between Anatase and Rutile TiO_2

Verena Pfeifer,[†] Paul Erhart,[‡] Shunyi Li,[†] Karsten Rachut,[†] Jan Morasch,[†] Joachim Brötz,[†] Philip Reckers,[†] Thomas Mayer,[†] Sven Rühle,[¶] Arie Zaban,[¶] Iván Mora Seró,[§] Juan Bisquert,[§] Wolfram Jaegermann,[†] and Andreas Klein*[,†]

[†]Institute of Materials Science, Technische Universität Darmstadt, D-64287 Darmstadt, Germany

[‡]Department of Applied Physics, Chalmers University of Technology, S-41296 Gothenburg, Sweden

[¶]Department of Chemistry, Bar Ilan University, 52900 Ramat Gan, Israel

[§]Departament de Física, University Jaume I, 12071 Castelló de la Plana, Spain

Supporting Information

ABSTRACT: Using photoelectron spectroscopy, the interface formation of anatase and rutile TiO_2 with RuO_2 and tin-doped indium oxide (ITO) is studied. It is consistently found that the valence band maximum of rutile is 0.7 ± 0.1 eV above that of anatase. The alignment is confirmed by electronic structure calculations, which further show that the alignment is related to the splitting of the energy bands formed by the O $2p_z$ lone-pair orbitals. The alignment can explain the different electron concentrations in doped anatase and rutile and the enhanced photocatalytic activity of mixed phase particles.

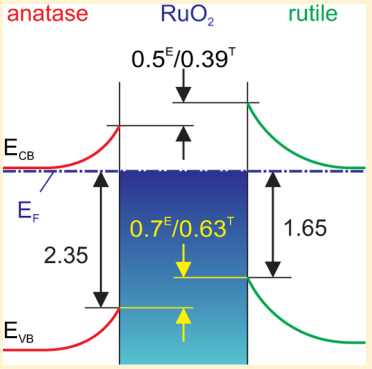

SECTION: Surfaces, Interfaces, Porous Materials, and Catalysis

After Fujishima and Honda[1] had reported on the photocatalytic activity of TiO_2, the influence of crystal structure on this property was investigated intensively.[2,3] Over the past 2 decades, it was commonly observed that mixed anatase/rutile systems show more favorable photocatalytic properties than pristine ones of either modification.[4−9] The synergistic effect of the mixed systems has been attributed to a built-in driving force for separation of photogenerated charge carriers. Such a driving force may result from either a built-in electric field or from energy barriers blocking charge transfer at the interface between anatase and rutile. The latter are described by the energy band alignment, which is well-studied for semiconductor interfaces.[10]

Connelly et al.[11] recently reviewed several models that are trying to explain the synergistic effect of mixed anatase/rutile systems. Well-known are the rutile sink model of Bickley et al.[4] and the rutile antenna model of Hurum et al.,[5] which place the band edges of rutile (energy band gap E_g = 3.0 eV[12]) in between the band edges of anatase (E_g = 3.2 eV[13]). Kavan et al.[14] performed electrochemical measurements that located the conduction band edge of anatase 0.2 eV above that of rutile, which corresponds to aligned valence band maxima. These models, however, were not able to convincingly account for the observed synergistic phenomena. Only recently, Deák et al.[15] as well as Scanlon et al.[16] found theoretical and experimental indications for an energy band alignment with valence and conduction band energies in rutile both located higher in energy than in anatase when brought into contact. With such a staggered energy band alignment at the anatase/rutile interface, photogenerated electrons will preferentially move to anatase due to its lower conduction band minimum energy E_{CB}, and holes will move to rutile due to its higher valence band maximum energy E_{VB}. Deák et al.[15] used the alignment of branch point energies[10] for their calculations. For oxides, though, it has been shown that due to a low density of induced interface states, the alignment of branch point energies does not necessarily yield proper results for the energy band alignment.[17]

In this work, further evidence for a staggered energy band alignment at the anatase/rutile interface is provided by X-ray photoelectron spectroscopy (XPS) measurements and density functional theory (DFT) calculations. XPS is a widely used technique for the determination of energy band alignments by interface experiments, in which one material is deposited stepwise onto the other.[10,17−19] There are various reasons why the performance of a direct interface experiment between anatase and rutile would be intricate. First, a TiO_2 thin film deposited stepwise onto a rutile substrate could hardly be forced into growing in anatase structure and vice versa. Furthermore, as the two modifications consist of identical elements, they show the same core-level emission lines in the

Received: October 7, 2013
Accepted: November 20, 2013
Published: November 20, 2013

   dx.doi.org/10.1021/jz402165b | J. Phys. Chem. Lett. 2013, 4, 4182−4187

XP spectra, and it would not be possible to distinguish between energy band offset and band bending effects.

For obtaining an energy band alignment between anatase and rutile, we have therefore studied the interface formation of anatase and rutile with two different contact materials, the low work function degenerately Sn-doped In_2O_3 (ITO, Φ = 4.5 eV[20]) and the high work function metallic RuO_2 (Φ = 6.1 eV[21]). With the use of oxide contact materials, a Fermi level pinning at the interface caused by deposition-induced interface defects[22] can be avoided. The energy band alignment between anatase and rutile is finally derived independently for both contact materials by making use of the transitivity rule, $\Delta E_{VB}(A/R) = \Delta E_{VB}(A/X) - \Delta E_{VB}(R/X)$, where A, R, and X represent anatase, rutile, and either ITO or RuO_2. In the case of metallic RuO_2, the Fermi level position is taken instead of the valence band maximum. ΔE_{VB} then corresponds to the hole Schottky barrier $\Phi_{B,p}$. The experimental investigations are supported by electronic structure calculations, which provide independent values for the band alignment and demonstrate that the higher valence band maximum of the rutile modification is related to the splitting of the energy bands of the nonbonding O $2p_z$ orbitals.

Polycrystalline anatase thin films on quartz glass as well as rutile bulk single crystals served as substrates for the experiments. Both substrates were free of contaminations and adsorbates due to either in situ deposition or annealing in oxygen atmosphere prior to the deposition of the contact material.[20] Comparing the XP valence band and core-level spectra of the different TiO_2 substrates, it is revealed that XPS can discriminate between anatase and rutile in two different ways, as illustrated in Figure 1.

The valence band structures of the two modifications differ considerably in shape on the one hand, as also observed by Scanlon et al.[16] On the other hand, the binding energy differences between the core-level emission lines and the valence band maxima ($\Delta E_{O\ 1s,VB}$ and $\Delta E_{Ti\ 2p,VB}$) are 0.45 ± 0.1 eV larger in rutile compared to those of anatase. The energies of the valence band maxima E_{VB} are determined here by the intersection of a linear extrapolation of the leading edge with the background intensity.[23] The binding energy differences $\Delta E_{CL,VB}$, which are material constants, are used below to derive the energy band alignment from the interface experiments using the Kraut method.[18] The large disparity of binding energy differences has been observed not only for the polycrystalline anatase and single-crystalline rutile samples but also for a number of other samples of the two modifications in poly- and single-crystalline structure (see Figure S2 in the Supporting Information). The $\Delta E_{CL,VB}$ are in good agreement with our electronic structure calculations (see Figure 3 and the Supporting Information).

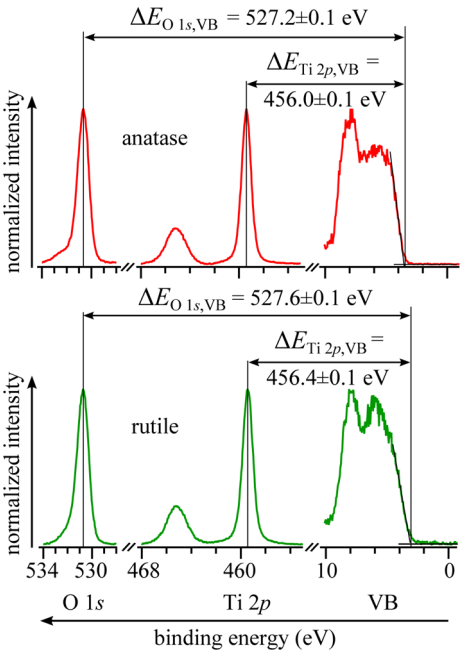

Figure 1. X-ray photoelectron spectra of the core-level emission lines O 1s and Ti 2p as well as the valence bands of anatase and rutile. The corresponding binding energy differences between the core levels and the valence band maxima are indicated.

Interface formation with RuO_2 and ITO was studied using stepwise deposition of the contact materials onto clean anatase and rutile substrates. After each incremental deposition step of the contact material, XP spectra were recorded without breaking vacuum to trace shifts in the binding energies of core-level emission lines and the evolution of peak shapes (see the Supporting Information). In all four experiments, the Ti core levels are successively attenuated, and either the Ru or the In and Sn core levels increase in intensity. No peak broadening or changes of line shape of the Ti 2p emissions are observed. Sample charging occurred during the rutile/RuO_2 experiment after surface cleaning and after the first deposition step. A charge neutralizer has been used during these measurements. With further RuO_2 deposition, and for all other samples, no charging occurred during measurement. The determination of barrier heights and band alignment is therefore not affected by charging effects.

The energies of the valence band maxima with respect to the Fermi energy ($E_F - E_{VB}$) are 3.2 ± 0.05 and 3.3 ± 0.05 eV for the uncoated anatase substrates and 2.9 ± 0.05 and 3.1 ± 0.05 eV for the uncoated rutile substrates, respectively. These values are very close to the band gaps of anatase and rutile and do therefore correspond to Fermi level positions near the conduction band minima. In the course of the experiments, the Ti 2p emission lines are progressively shifted toward lower binding energies with increasing coverage. From the Ti 2p binding energies, the change of E_{VB} is directly obtained using the binding energy differences $\Delta E_{Ti\ 2p,VB}$ (Figure 1). The obtained E_{VB} as a function of coverage for all four experiments are displayed in Figure 2.

For both substrates, the shifts of the Ti 2p binding energies, which correspond to band bending in the substrates, are larger for RuO_2 deposition compared to the deposition of ITO. This has to be expected from the larger work function of RuO_2. It is noted, however, that the difference of the Fermi level positions at the RuO_2 and ITO interfaces is smaller than the difference of their work functions. This is caused by interface dipole contributions to the energy band alignment.[24] In all four experiments, the binding energy shifts saturate after 1−2 nm overlayer thickness, indicating that the electronic barrier is completed before the substrate emissions are fully attenuated by the deposited film. The saturation values of $E_F - E_{VB}$ are 0.7 ± 0.1 eV higher for anatase compared to those for rutile. This is the case for both contact materials, indicating transitivity of energy band alignment. Further support for the transitivity of band alignment can be found in the Supporting Information.

Applying the transitivity rule, the different Fermi level positions at the interface can be assigned to an offset between

dx.doi.org/10.1021/jz402165b | J. Phys. Chem. Lett. 2013, 4, 4182−4187

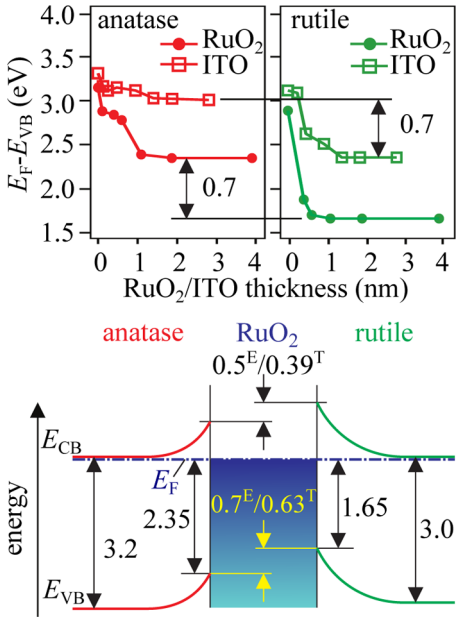

Figure 2. (top) Evolution of the Ti 2p core-level binding energies with increasing RuO_2/ITO film thickness on anatase and rutile substrates. The constant $\Delta E_{Ti\ 2p,VB}$ are subtracted, whereby the evolution of E_{VB} is obtained. (bottom) Energy band diagrams for anatase/RuO_2 and rutile/RuO_2 interfaces derived from the evolution of the binding energy. The Fermi level positions in the bulk and at the interface are derived from the upper graph from the substrates and after saturation of energy shifts, respectively. The band alignment at the rutile/anatase interface is obtained using transitivity from the figure by omitting the central RuO_2 layer and the band bendings. The resulting valence and conduction band discontinuities at the rutile/anatase interface derived from the photoemission experiment are indicated by superscript E, and those from DFT calculations are indicated by superscript T.

the valence band edges of anatase and rutile of ΔE_{VB} = 0.7 ± 0.1 eV, with the VBM of rutile being higher than that of anatase (see Figure 2). Using literature values for the band gaps of rutile and anatase,[12,13] a conduction band discontinuity of ΔE_{CB} = 0.5 ± 0.1 eV results. This means that the valence and the conduction band edges of rutile are both higher in energy than their corresponding counterparts in anatase in direct contact of the two materials. This corresponds to a staggered type-II energy band alignment between anatase and rutile close to those reported by Deák et al. and by Scanlon et al.[15,16]

In previous work, it has been suggested that the valence band discontinuity between oxides is small when the valence band states are predominantly formed by O 2p states (so-called common anion rule alignment).[17] This was concluded from the observation that higher-lying valence bands have only been observed when cation orbitals contribute to the valence band states. Examples are $PbTiO_3$,[25] Bi_2O_3,[26] and $BiFeO_3$[26] with 6s orbitals or Fe_2O_3[26] and Cu_2O,[27] with 3d orbitals contributing to the valence band states. The common anion rule[28] can be traced back to the fact that in the bond orbital approximation of LCAO theory (linear combination of atomic orbitals), the valence band maximum energy of tetrahedrally coordinated semiconductors depends predominantly on the energy of the anion p orbital.[17,29] The rutile modification of TiO_2 is a clear exception from the common anion rule alignment as the higher valence band maximum cannot be related to contributions of Ti states to the valence bands. It is therefore important to understand whether this exception is caused by the presence of strong interface dipoles or by a particular bonding configuration.

To gain further insight regarding the origin of the band discontinuity at the rutile/anatase interface, we analyzed the electronic structure on a DFT level (see the Experimental Section and the Supporting Information for details). Comparison of the density of states (DOS) of rutile and anatase (see Figure 3a) yields a valence band discontinuity of 0.63 eV and a conduction band discontinuity of 0.39 eV, both in very good agreement with the experimentally determined values (see Figure 2). Further inspection of the valence band structure shows that for the most part, the DOSs of rutile and anatase are very similar except for the appearance of "tails" at both the valence band top and bottom in the case of rutile. This suggests that the valence band offset is intimately related to these features.

The band structure of rutile shown in Figure 3b demonstrates that the tails originate from a pronounced splitting of the topmost and bottommost levels in the vicinity of the Γ point, which is entirely absent in anatase (see Figure S12 in the Supporting Information). The electronic origin of this feature can be clarified with the help of a Wannier function analysis,[30−32] which yields one sp^2- and one p_z-like orbital for each oxygen atom, as can be seen in Figure 3c,d. The three lobes of the sp^2 orbital are oriented along the O−Ti bonds, whereas the p_z-like orbital is oriented perpendicular to the sp^2 plane. The projection of the band structure on this set of states yields the relative admixture illustrated by the color coding in Figure 3b. This analysis reveals that the topmost valence band near Γ, where a pronounced separation from the other valence states occurs, is virtually exclusively of p_z character and thus can be interpreted as a lone-pair orbital, in agreement with resonant photoemission experiments.[33] The lone-pair orbital does not participate in the O−Ti bond, and the splitting of the level can consequently be understood in terms of a LCAO picture.[34] The σ-like overlap of the lone-pair orbitals of neighboring O atoms explains the downward dispersion of the band away from the center of the Brillouin zone Γ.

The Wannier basis generated in the same fashion for anatase resembles the one for rutile insofar that a decomposition into sp^2- and p_z-like orbitals is obtained (see Figure S12 in the Supporting Information). Unlike the case of rutile, however, the p_z-like orbital does not play a prominent role near the valence band edges, and the band structure also does not exhibit a splitting of states around the Γ point. The difference between the two types of behavior originating from the respective orientation of the ensemble of p_z-like orbitals in the two different crystal structures is clearly seen in a comparison of the Wannier function analysis (see Figures S11(f) and S12(f) in the Supporting Information). In rutile, the p_z-like orbitals are much closer to each other, suggesting stronger interaction and overlap, which results in a larger splitting of the corresponding energy bands and consequently in a higher valence band maximum energy and the appearance of the tail at the top of the valence band. We have thus established a direct connection between the crystal structures of rutile and anatase, their electronic structures and, most significantly in the present context, the valence band offset between the two phases.

The concept of doping limits of semiconductors states that limits of the Fermi level position are on a similar energy level with a proper energy band alignment of materials.[35−37] Such a behavior has been explicitly demonstrated using Fermi level measurements and energy band alignment for (Ba,Sr)TiO_3 and

dx.doi.org/10.1021/jz402165b | J. Phys. Chem. Lett. 2013, 4, 4182−4187

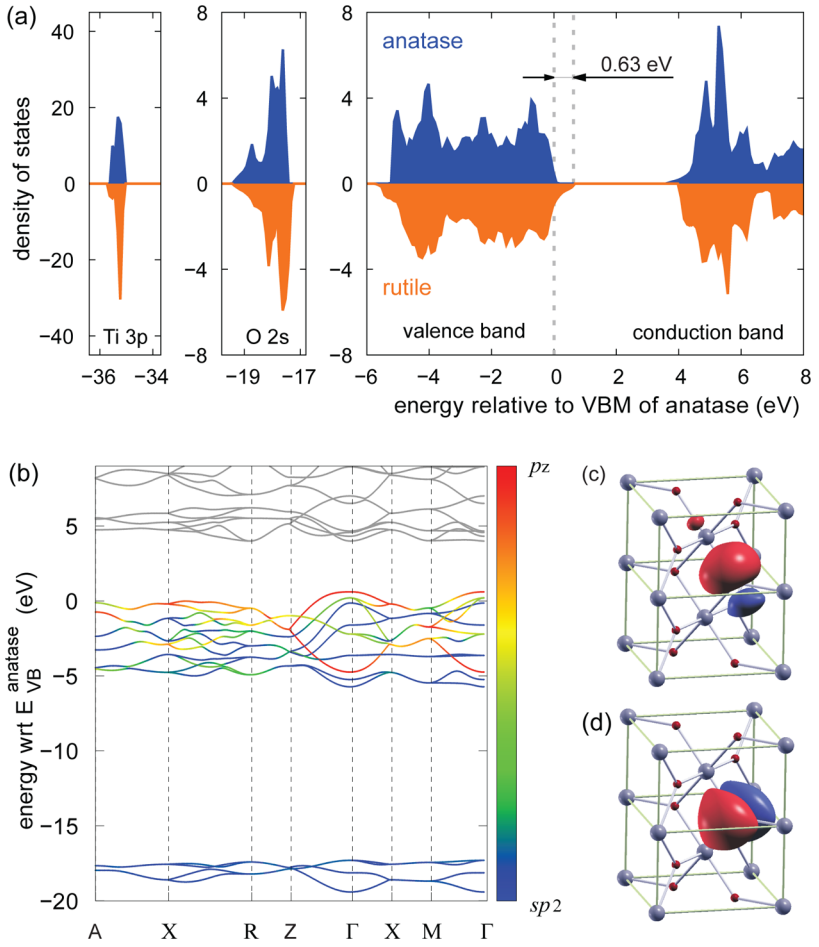

Figure 3. (a) Comparison of the DOSs of rutile and anatase. The energy scales have been aligned based on the electrostatic potential at the Ti cores. (b) Band structure of rutile where the color scale indicates the respective admixture of oxygen-centered (c) sp^2- and (d) p_z-like orbitals. In (c), only one of the three individual Wannier functions that contribute to the sp^2-like orbital is shown. The remaining lobes are oriented along the other two O−Ti bonds.

$Pb(Zr,Ti)O_3$.[25] A lower conduction band minimum would therefore allow a higher electron concentration. Within this concept, the obtained alignment with a lower conduction band in anatase agrees with the higher electron concentrations, which can be achieved in anatase, for example, by Nb doping compared to rutile.[38]

The presented experiments and electronic structure calculations consistently reveal a staggered energy band alignment between anatase and rutile, with the valence band maximum of rutile at 0.7 ± 0.1 eV (experimental) or 0.63 eV (theoretical) above that of anatase. Transitivity of energy band alignment has been demonstrated explicitly using two different conducting oxides as contact materials, which gives confidence that the experimentally determined alignment is not corrupted by defect-induced Fermi level pinning.[22,39] The obtained band alignments support previous studies by Deák et al.[15] and Scanlon et al.[16] Moreover, the analysis of the electronic structure shows that the higher valence band maximum of rutile is caused by the stronger overlap between the O $2p_z$ orbitals in rutile compared to those in anatase, leading to a substantial splitting of the resulting energy bands. The staggered band alignment explains the enhanced photocatalytic activity of mixed phase TiO_2 particles[4−9] as it provides a driving force for separation of photoexcited charge carriers. Within the concept of general doping limits,[35−37] the staggered alignment of the energy bands also explains the higher electron concentrations, which have been obtained with anatase compared to rutile TiO_2.[38]

EXPERIMENTAL SECTION

Sample preparation as well as all XPS measurements were performed using the Darmstadt Integrated System for Materials Research (DAISY-MAT).[37] This system permits thin film deposition by magnetron sputtering and characterization via monochromatic XPS (Physical Electronics PHI5700, Al K_α, $h\nu$ = 1486.6 eV) without breaking vacuum. Binding energies are recorded with respect to the Fermi energy, which is calibrated using a sputter-cleaned Ag foil.

Thin films of TiO_2 and RuO_2 were deposited using reactive magnetron sputtering from metallic Ti and Ru targets, respectively. ITO deposition was performed by radio frequency magnetron sputtering from a ceramic ITO (10 wt % SnO_2) target. Rutile single crystals with a (001) orientation (CrysTec, Germany) were used. To prevent charging of the poorly conducting anatase and rutile substrates during the XPS measurements, a 100 nm thick platinum film with a central hole of 1 mm diameter was deposited onto the surface.[40] Charging occurred only for one of the rutile crystals after adsorbate removal and after the very first RuO_2 deposition step. This charging does not affect the determination of the band

dx.doi.org/10.1021/jz402165b | J. Phys. Chem. Lett. 2013, 4, 4182−4187

alignment, which is derived from spectra with thicker overlayers, where no charging occurred. Before stepwise deposition of the contact materials, the surfaces were cleaned from adsorbates by heating in an oxygen atmosphere (p = 0.5 Pa, T = 500 °C, t = 3.5 h).[20]

Calculations were carried out within DFT using the projector augmented wave method[41,42] as implemented in the Vienna ab initio simulation package.[43−46] Electronic states down to the Ti 3p and O 2s shells were treated as part of the valence. All calculations were carried out at the experimentally determined lattice parameters[47] and employed a plane wave cutoff energy of 400 eV as well as a Γ-centered 6 × 6 × 6 k-point mesh. A range-separated hybrid exchange−correlation (XC) functional (HSE06)[48] was employed that has been found in earlier studies[15,16] to produce band structures and energy gaps in very good agreement with experiment and G_0W_0 calculations.[49,50] The results obtained with other XC functionals are similar, as shown in the Supporting Information. The energy scales of rutile and anatase were aligned based on the electrostatic potential at the Ti sites. On the basis of convergence tests, we estimate the numerical error of the computed band offsets to be less than 50 meV. Maximally localized Wannier functions[30] were employed to interpolate the eigen energy spectra on very dense k-point grids[31,32] and to interpret the nature of chemical bonding in rutile and anatase. Wannier functions were rendered with the XCRYSDEN software.[51]

■ ASSOCIATED CONTENT

Supporting Information

Experimental details, spectra of the interface experiments, details and extensive description of electronic structure, and wave function analysis are presented. This material is available free of charge via the Internet at http://pubs.acs.org.

■ AUTHOR INFORMATION

Corresponding Author

*E-mail: aklein@surface.tu-darmstadt.de.

Notes

The authors declare no competing financial interest.

■ ACKNOWLEDGMENTS

This work has been supported by the German Science Foundation (DFG) under the collaborative research center SFB595 "Electrical Fatigue of Functional Materials" and the European Commission under FP7 AllOxidePV project "Novel Composite Oxides by Combinatorial Material Synthesis for Next Generation All-Oxide-Photovoltaics", Number 309018. P.E. acknowledges funding from the European Research Council via a Marie Curie Career Integration Grant and the "Area of Advance — Materials Science" at Chalmers University of Technology. Computer time allocations by the Swedish National Infrastructure for Computing are gratefully acknowledged. We further thank Bruce A. Parkinson for providing a single crystal of anatase.

■ REFERENCES

(1) Fujishima, A.; Honda, K. Electrochemical Photolysis of Water at a Semiconductor Electrode. *Nature* **1972**, *238*, 37−38.

(2) Tanaka, K.; Capule, M. F. V.; Hisanaga, T. Effect of Crystallinity of TiO_2 on Its Photocatalytic Action. *Chem. Phys. Lett.* **1991**, *187*, 73−76.

(3) Nishimoto, S.; Ohtani, B.; Kajiwara, H.; Kagiya, T. Correlation of the Crystal Structure of Titanium Dioxide Prepared from Titanium Tetra-2-propoxide with the Photocatalytic Activity for Redox Reactions in Aqueous Propan-2-ol and Silver Salt Solutions. *J. Chem. Soc., Faraday Trans. 1* **1985**, *81*, 61−68.

(4) Bickley, R. I.; Gonzalez-Carreno, T.; Lees, J. S.; Palmisano, L.; Tilley, R. J. A Structural Investigation of Titanium Dioxide Photocatalysts. *J. Solid State Chem.* **1991**, *92*, 178−190.

(5) Hurum, D. C.; Agrios, A. G.; Gray, K. A.; Rajh, T.; Thurnauer, M. C. Explaining the Enhanced Photocatalytic Activity of Degussa P25 Mixed-Phase TiO_2 Using EPR. *J. Phys. Chem. B* **2003**, *107*, 4545−4549.

(6) Ohno, T.; Sarukawa, K.; Tokieda, K.; Matsumura, M. Morphology of a TiO_2 Photocatalyst (Degussa, P-25) Consisting of Anatase and Rutile Crystalline Phases. *J. Catal.* **2001**, *203*, 82−86.

(7) Ohno, T.; Tokieda, K.; Higashida, S.; Matsumura, M. Synergism Between Rutile and Anatase TiO_2 Particles in Photocatalytic Oxidation of Naphthalene. *Appl. Catal., A* **2003**, *244*, 383−391.

(8) Li, G.; Chen, L.; Graham, M. E.; Gray, K. A. A Comparison of Mixed Phase Titania Photocatalysts Prepared by Physical and Chemical Methods: The Importance of the Solid−Solid Interface. *J. Mol. Catal. A: Chem.* **2007**, *275*, 30−35.

(9) Kho, Y. K.; Iwase, A.; Teoh, W. Y.; Mädler, L.; Kudo, A.; Amal, R. Photocatalytic H_2 Evolution over TiO_2 Nanoparticles. The Synergistic Effect of Anatase and Rutile. *J. Phys. Chem. C* **2010**, *114*, 2821−2829.

(10) Yu, E. T.; McCaldin, J. O.; McGill, T. C. Band Offsets in Semiconductor Heterojunctions. *Solid State Physics* **1992**, *46*, 1−146.

(11) Connelly, K. A.; Idriss, H. The Photoreaction of TiO_2 and Au/TiO_2 Single Crystal and Powder Surfaces with Organic Adsorbates. Emphasis on Hydrogen Production from Renewables. *Green Chem.* **2012**, *14*, 260−280.

(12) Pascual, J.; Camassel, J.; Mathieu, H. Fine Structure in the Intrinsic Absorption Edge of TiO_2. *Phys. Rev. B* **1978**, *18*, 5606−5614.

(13) Tang, H.; Berger, H.; Schmid, P.; Lévy, F.; Burri, G. Photoluminescence in TiO_2 Anatase Single Crystals. *Solid State Commun.* **1993**, *87*, 847−850.

(14) Kavan, L.; Grätzel, M.; Gilbert, S. E.; Klemenz, C.; Scheel, H. J. Electrochemical and Photoelectrochemical Investigation of Single-Crystal Anatase. *J. Am. Chem. Soc.* **1996**, *118*, 6716−6723.

(15) Deák, P.; Aradi, B.; Frauenheim, T. Band Lineup and Charge Carrier Separation in Mixed Rutile−Anatase Systems. *J. Phys. Chem. C* **2011**, *115*, 3443−3446.

(16) Scanlon, D. O.; Dunnill, C. W.; Buckeridge, J.; Shevlin, S. A.; Logsdail, A. J.; Woodley, S. M.; Catlow, C. R. A.; Powell, M. J.; Palgrave, R. G.; Parkin, I. P.; Watson, G. W.; Keal, T. W.; Sherwood, P.; Walsh, A.; Sokol, A. A. Band Alignment of Rutile and Anatase TiO_2. *Nat. Mater.* **2013**, *12*, 798−801.

(17) Klein, A. Energy Band Alignment at Interfaces of Semiconducting Oxides: A Review of Experimental Determination Using Photoelectron Spectroscopy and Comparison with Theoretical Predictions by the Electron Affinity Rule, Charge Neutrality Levels, and the Common Anion Rule. *Thin Solid Films* **2012**, *520*, 3721−3728.

(18) Waldrop, J. R.; Grant, R. W.; Kowalczyk, S. P.; Kraut, E. A. Measurement of Semiconductor Heterojunction Band Discontinuities by X-ray Photoemission Spectroscopy. *J. Vac. Sci. Technol., A* **1985**, *3*, 835−841.

(19) Chambers, S.; Ohsawa, T.; Wang, C.; Lyubinetsky, I.; Jaffe, J. Band Offsets at the Epitaxial Anatase TiO_2/n-$SrTiO_3$(001) Interface. *Surf. Sci.* **2009**, *603*, 771−780.

(20) Gassenbauer, Y.; Schafranek, R.; Klein, A.; Zafeiratos, S.; Hävecker, M.; Knop-Gericke, A.; Schlögl, R. Surface States, Surface Potentials and Segregation at Surfaces of Tin-Doped In_2O_3. *Phys. Rev. B* **2006**, *73*, 245312/1−245312/11.

(21) Schafranek, R.; Schaffner, J.; Klein, A. In-Situ Photoelectron Study of the (Ba,Sr)TiO_3/RuO_2 Contact Formation. *J. Eur. Ceram. Soc.* **2010**, *30*, 187−192.

(22) Chen, F.; Schafranek, R.; Wu, W.; Klein, A. Reduction Induced Fermi Level Pinning at the Interfaces between Pb(Zr,Ti)O_3 and Pt, Cu and Ag Metal Electrodes. *J. Phys. D: Appl. Phys.* **2011**, *44*, 255301/1−7.

(23) Chambers, S. A.; Droubay, T.; Kaspar, T. C.; Gutowski, M. Experimental Determination of Valence Band Maxima for $SrTiO_3$, TiO_2, and SrO and the Associated Valence Band Offsets with Si(001). *J. Vac. Sci. Technol. B* **2004**, *22*, 2205−2215.
(24) Mönch, W. On the Electric-Dipole Contribution to the Valence-Band Offsets in Semiconductor−Oxide Heterostructures. *Appl. Phys. Lett.* **2007**, *91*, 042117.
(25) Schafranek, R.; Li, S.; Chen, F.; Wu, W.; Klein, A. $PbTiO_3$/$SrTiO_3$ Interface: Energy Band Alignment and its Relation to the Limits of Fermi Level Variation. *Phys. Rev. B* **2011**, *84*, 045317/1−045317/7.
(26) Li, S.; Morasch, J.; Klein, A.; Chirila, C.; Pintilie, L.; Jia, L.; Ellmer, K.; Naderer, M.; Reichmann, K.; Gröting, M.; Albe, K. Influence of Orbital Contributions to the Valence Band Alignment of Bi_2O_3, Fe_2O_3, $BiFeO_3$, and $Bi_{0.5}Na_{0.5}TiO_3$. *Phys. Rev. B* **2013**, *88*, 045428/1−045428/12.
(27) Deuermeier, J.; Gassmann, J.; Brötz, J.; Klein, A. Reactive Magnetron Sputtering of Cu_2O: Dependence on Oxygen Pressure and Interface Formation with Indium Tin Oxide. *J. Appl. Phys.* **2011**, *109*, 113704/1−113704/7.
(28) McCaldin, J. O.; McGill, T. C.; Mead, C. A. Correlation for III−V and II−VI Semiconductors of the Au Schottky Barrier Energy with Anion Electronegativity. *Phys. Rev. Lett.* **1976**, *36*, 56−58.
(29) Harrison, W. A.; Tersoff, J. Tight-Binding Theory of Heterojunction Band Lineups and Interface Dipoles. *J. Vac. Sci. Technol., B* **1986**, *4*, 1068−1073.
(30) Marzari, N.; Mostofi, A. A.; Yates, J. R.; Souza, I.; Vanderbilt, D. Maximally Localized Wannier Functions: Theory and Applications. *Rev. Mod. Phys.* **2012**, *84*, 1419−1475.
(31) Mostofi, A. A.; Yates, J. R.; Lee, Y.-S.; Souza, I.; Vanderbilt, D.; Marzari, N. Wannier90: A Tool for Obtaining Maximally-Localised Wannier Functions. *Comput. Phys. Commun.* **2008**, *178*, 685−699.
(32) Åberg, D.; Erhart, P.; Crowhurst, J.; Zaug, J. M.; Goncharov, A. F.; Sadigh, B. Pressure-Induced Phase Transition in the Electronic Structure of Palladium Nitride. *Phys. Rev. B* **2010**, *82*, 104116.
(33) Thomas, A. G.; et al. Comparison of the Electronic Structure of Anatase and Rutile TiO_2 Single-Crystal Surfaces Using Resonant Photoemission and X-ray Absorption Spectroscopy. *Phys. Rev. B* **2007**, *75*, 035105/1−035105/12.
(34) Hoffmann, R. How Chemistry and Physics Meet in the Solid State. *Angew. Chem., Int. Ed. Engl.* **1987**, *26*, 846−878.
(35) Zhang, S. B.; Wei, S.-H.; Zunger, A. A Phenomenological Model for Systematization and Prediction of Doping Limits in II−VI and I−III−VI_2 Compounds. *J. Appl. Phys.* **1998**, *83*, 3192−3196.
(36) Robertson, J.; Clark, S. J. Limits to Doping in Oxides. *Phys. Rev. B* **2011**, *83*, 075205/1−075205/7.
(37) Klein, A. Transparent Conducting Oxides: Electronic Structure−Property Relationship from Photoelectron Spectroscopy with In Situ Sample Preparation. *J. Am. Ceram. Soc.* **2013**, *96*, 331−345.
(38) Hitosugi, T.; Ueda, A.; Nakao, S.; Yamada, N.; Furubayashi, Y.; Hirose, Y.; Shimada, T.; Hasegawa, T. Fabrication of Highly Conductive $Ti_{1-x}Nb_xO_2$ Polycrystalline Films on Glass Substrates via Crystallization of Amorphous Phase Grown by Pulsed Laser Deposition. *Appl. Phys. Lett.* **2007**, *90*, 212106/1−212106/3.
(39) Bayer, T. J.; Wachau, A.; Fuchs, A.; Deuermeier, J.; Klein, A. Atomic Layer Deposition of Al_2O_3 onto Sn-Doped In_2O_3: Absence of Self-Limited Adsorption during Initial Growth by Oxygen Diffusion from the Substrate and Band Offset Modification by Fermi Level Pinning in Al_2O_3. *Chem. Mater.* **2012**, *24*, 4503−4510.
(40) Chen, F.; Schafranek, R.; Wachau, A.; Zhukov, S.; Glaum, J.; Granzow, T.; von Seggern, H.; Klein, A. Barrier Heights, Polarization Switching and Electrical Fatigue in $Pb(Zr,Ti)O_3$ Ceramics with Different Electrodes. *J. Appl. Phys.* **2010**, *108*, 104106/1−104106/7.
(41) Blöchl, P. E. Projector Augmented-Wave Method. *Phys. Rev. B* **1994**, *50*, 17953−17979.
(42) Kresse, G.; Joubert, D. From Ultrasoft Pseudopotentials to the Projector Augmented-Wave Method. *Phys. Rev. B* **1999**, *59*, 1758−1775.
(43) Kresse, G.; Hafner, J. Ab Initio Molecular Dynamics for Liquid Metals. *Phys. Rev. B* **1993**, *47*, 558−561.
(44) Kresse, G.; Hafner, J. Ab Initio Molecular-Dynamics Simulation of the Liquid−Metal−Amorphous−Semiconductor Transition in Germanium. *Phys. Rev. B* **1994**, *49*, 14251−14269.
(45) Kresse, G.; Furthmüller, J. Efficient Iterative Schemes for Ab Initio Total-Energy Calculations Using a Plane-Wave Basis Set. *Phys. Rev. B* **1996**, *54*, 11169−11186.
(46) Kresse, G.; Furthmüller, J. Efficiency of Ab-Initio Total Energy Calculations for Metals and Semiconductors Using a Plane-Wave Basis Set. *Comput. Mater. Sci.* **1996**, *6*, 15−50.
(47) Howard, C. J.; Sabine, T. M.; Dickson, F. Structural and Thermal Parameters for Rutile and Anatase. *Acta Crystallogr., Sect. B* **1991**, *47*, 462−468.
(48) Heyd, J.; Scuseria, G.; Ernzerhof, M. Hybrid Functionals Based on a Screened Coulomb Potential. *J. Chem. Phys.* **2003**, *118*, 8207−8215. (b) Heyd, J.; Scuseria, G.; Ernzerhof, M. Erratum: Hybrid Functionals Based on a Screened Coulomb Potential. *J. Chem. Phys.* **2006**, *124*, 219906/1.
(49) Kang, W.; Hybertsen, M. S. Quasiparticle and Optical Properties of Rutile and Anatase TiO_2. *Phys. Rev. B* **2010**, *82*, 085203/1−085203/11.
(50) Chiodo, L.; Garca-Lastra, J. M.; Iacomino, A.; Ossicini, S.; Zhao, J.; Petek, H.; Rubio, A. Self-Energy and Excitonic Effects in the Electronic and Optical Properties of TiO_2 Crystalline Phases. *Phys. Rev. B* **2010**, *82*, 045207/1−045207/12.
(51) Kokalj, A. Computer Graphics and Graphical User Interfaces as Tools in Simulations of Matter at the Atomic Scale. *Comput. Mater. Sci.* **2003**, *28*, 155−168 ; code available from http://www.xcrysden.org/.